Vaiyapuri, T, Liyakathunisa, Alaskar, H, Parvathi, R, Pattabiraman, V and Hussain, A

Cat Swarm Optimization-Based Computer-Aided Diagnosis Model for Lung Cancer Classification in Computed Tomography Images

applied sciences

MDPI

Article

Cat Swarm Optimization-Based Computer-Aided Diagnosis Model for Lung Cancer Classification in Computed Tomography Images

Thavavel Vaiyapuri [1], Liyakathunisa [2], Haya Alaskar [1,*], Ramasubramanian Parvathi [3], Venkatasubbu Pattabiraman [3] and Abir Hussain [4,5]

[1] Department of Computer Science, College of Computer Engineering and Sciences, Prince Sattam Bin Abdulaziz University, Al Kharj 16278, Saudi Arabia; t.thangam@psau.edu.sa
[2] Department of Computer Science, College of Computer Science and Engineering, Taibah University, Madinah 42353, Saudi Arabia; lansari@taibahu.edu.sa
[3] School of Computing Science and Engineering, Vellore Institute of Technology, Chennai 600127, India; parvathi.r@vit.ac.in (R.P.); pattabiraman.v@vit.ac.in (V.P.)
[4] Department of Electrical Engineering, University of Sharjah, Sharjah P.O. Box 27272, United Arab Emirates; a.hussain@ljmu.ac.uk
[5] Department of Computer Science, Liverpool John Moores University, Liverpool L3 3AF, UK
* Correspondence: h.alaskar@psau.edu.sa

Abstract: Lung cancer is the most significant cancer that heavily contributes to cancer-related mortality rate, due to its violent nature and late diagnosis at advanced stages. Early identification of lung cancer is essential for improving the survival rate. Various imaging modalities, including X-rays and computed tomography (CT) scans, are employed to diagnose lung cancer. Computer-aided diagnosis (CAD) models are necessary for minimizing the burden upon radiologists and enhancing detection efficiency. Currently, computer vision (CV) and deep learning (DL) models are employed to detect and classify the lung cancer in a precise manner. In this background, the current study presents a cat swarm optimization-based computer-aided diagnosis model for lung cancer classification (CSO-CADLCC) model. The proposed CHO-CADLCC technique initially pre-process the data using the Gabor filtering-based noise removal technique. Furthermore, feature extraction of the pre-processed images is performed with the help of NASNetLarge model. This model is followed by the CSO algorithm with weighted extreme learning machine (WELM) model, which is exploited for lung nodule classification. Finally, the CSO algorithm is utilized for optimal parameter tuning of the WELM model, resulting in an improved classification performance. The experimental validation of the proposed CSO-CADLCC technique was conducted against a benchmark dataset, and the results were assessed under several aspects. The experimental outcomes established the promising performance of the CSO-CADLCC approach over recent approaches under different measures.

Keywords: computer-aided diagnosis; deep learning; intelligent models; healthcare; cat swarm optimization; computer vision

Citation: Vaiyapuri, T.; Liyakathunisa; Alaskar, H.; Parvathi, R.; Pattabiraman, V.; Hussain, A. Cat Swarm Optimization-Based Computer-Aided Diagnosis Model for Lung Cancer Classification in Computed Tomography Images. *Appl. Sci.* **2022**, *12*, 5491. https://doi.org/10.3390/app12115491

Academic Editors: Cecilia Di Ruberto, Andrea Loddo and Lorenzo Putzu

Received: 18 March 2022
Accepted: 17 May 2022
Published: 28 May 2022

1. Introduction

Currently, lung cancer is the leading cause of cancer-related mortality across the globe, while in underdeveloped and developed countries, it records a low survival rate after diagnosis [1]. Based on the present statistics, the 5-year survival rate is around 16%; it is predicted that there will be 12 million cancer-related deaths per year by the end of 2020, with highest percentage of these being lung cancer-related deaths [2]. When nodules are diagnosed at an early stage, the survival rate can be enhanced. Lung nodules are abnormally growing tissues that represent lung cancer. Typically, the nodules are spherical or round in shape, with a diameter of 30 mm. Medical images are captured using different imaging

modalities [3]. Amongst others, computed tomography (CT) is a basic imaging approach for screening lung nodules, whereas other available approaches are of less significance [4].

The computer-aided detection (CAD) technique assists in early diagnoses of lung cancer [5]. The primary objective of CAD is to recognize and extract the regions of interest (ROI) from the images attained using imaging modalities. The segmentation of lung tissue from chest images during the preprocessing stage is emerging in the CAD scheme, so as to reduce the searching region for lung nodules [6]. Then, the other essential steps in this process are the segmentation and detection of lung nodules in the presented searching space. Finally, the nodules are classified as benign or malignant [7]. In the CAD technique, the final phase is the main element for diagnosis and recognition of lung nodules from CT. In CAD systems for diagnosis, a classification module classifies the nodule candidates, recognized during the preceding phase, into nodules or non-nodules (i.e., based on their anatomic structure). Further, the CAD scheme for diagnoses (also known as CADx) categorizes the diagnosed nodules (whether by a radiologist or a computer) into benign or malignant [8].

CAD is a computerized process for pathological diagnoses of malignant tumors, and it belongs to the class of artificial intelligence (AI). This technique helps in analyzing tumor lesions through medical image processing technique and other possible biochemical and physiological methods integrated with calculation and analysis. In the healthcare sector, AI transforms qualitative subjective image data into quantitative objective image data, and assists the clinician in increasing the precision of medical decision-making [9]. Deep learning (DL) is a subdivision of AI which automatically extracts the discriminatory data features from datasets. With simple extraction method, the performance can be adapted systematically and easily [10].

Among the available DL models, the convolutional neural network (CNN) model has shown better performance than other DL architectures. Many machine learning (ML) models necessitate the investigation of relationship of data with class labels in order to extract the optimal features for classification. The outcome of the classifier is decided by the features being chosen. Lung cancer classification using the CNN model provides better results than other DL models such as auto encoders; as such, many studies have started to focus on enhancing the CNN model. It has the ability to classify biomedical images with improved accuracy over handcrafted features such as histogram, shape, texture, and so on. Numerous ML models, specifically DL models, have been employed for lung cancer classification. Several ML algorithms, for instance the deep learning algorithm, have been used to accomplish this task, but without guaranteed accuracy. Therefore, there is still room for improvement.

In this background, the current research article presents the cat swarm optimization-based computer-aided diagnosis model for lung cancer classification (CSO-CADLCC) model. In the proposed CHO-CADLCC technique, first the data undergo pre-processing using the Gabor filtering-based noise removal process. Moreover, feature extraction of the pre-processed images is performed using the NASNetLarge model. Furthermore, the CSO algorithm with weighted extreme learning machine (WELM) model is exploited for lung nodule classification. Finally, the CSO algorithm is utilized for optimal parameter tuning of the WELM model, thereby producing improved classification performance. The experimental validation of the proposed CSO-CADLCC technique was conducted against a benchmark dataset, and the results were assessed under several aspects.

2. Related Works

Hu et al. [11] developed a CAD method to categorize nodules into benign and malignant ground glass nodules (GGNs), and combined radiomics imaging and deep learning features to enhance the classification accuracy. On the basis of pretrained U-Net, the proposed method can be utilized as a transfer learning method to construct a deep neural network (DNN) so as to distinguish benign and malignant GGNs. In the literature [12], a deep convolution neural network (DCNN)-based fuzzy feature technique was developed to handle the difficulty of reading lung CT images. Then, the effect of distinct methods

to identify the lung tumor was investigated by altering feature dimension, depth of the network, and convolutional kernel size.

Guo et al. [13] presented a lung cancer diagnosis method based on CT scan imaging for the recognition of the disease. The presented technique employed a consecutive method to accomplish the outcome. Subsequently, two well-organized classifiers i.e., CNN and feature-based methods, were employed. Initially, the CNN classification was improved by a recently developed optimizer named the 'Harris hawk optimizer'. Ali et al. [14] presented a decision level fusion method to improve the efficiency of the CAD scheme for the classification of lung nodules. Firstly, it estimates the accuracy of Support Vector Machine (SVM) and AdaBoostM2 approaches on deep feature from advanced transferable architecture.

Mastouri et al. [15] presented a novel classifier method termed bilinear CNN (BCNN) for the classification of lung nodules on CT images. The presented BCNN technique has a two-stream CNNs (VGG16 and VGG19) for feature extraction, along with an SVM technique for false positive reduction. A series of experiments was conducted by establishing bilinear vector feature extraction in three BCNN combinations. Shaffie et al. [16] presented a novel CAD method for lung cancer analysis in chest CT scans. The presented method removes two distinct types of features, such as appearance and shape features. In the literature [17], CAD models that are dependent upon DL techniques were verified for their efficacy in the automatic recognition and classification of lung cancer. The advanced technique i.e., multiple view convolution recurrent neural network (MV-CRecNet) was presented not only by exploiting shape, size, and cross-slice differences, but also by learning to recognize lung cancer nodule in CT scan. The multi-view method enabled optimum generalization and learning of robust features.

3. The Proposed Model

In this study, a new CSO-CADLCC model has been developed for the identification and classification of lung cancer using CT images. The presented CSO-CADLCC model comprises of a GF technique to eradicate the noise at preliminary stage. Then, a feature extraction process is carried out on the pre-processed images using a NASNetLarge model. Following on, the WELM model receives the feature vectors and classifies the CT images under distinct classes. In order to fine-tune the parameters involved in WELM model, a CSO algorithm is utilized. Figure 1 depicts the overall block diagram of the CSO-CADLCC technique.

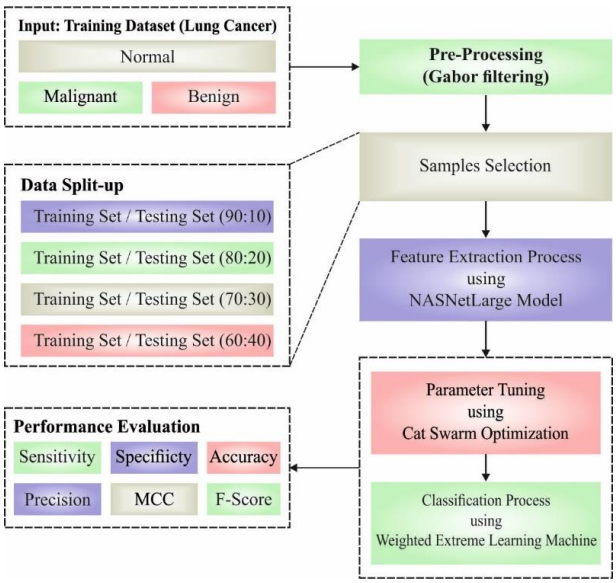

Figure 1. Overall block diagram of the CSO-CADLCC technique.

3.1. Image Pre-Processing: GF Technique

GF, a bandpass filter, is effectively employed for different machine vision and image processing applications [18]. A 2D Gabor function is an oriented complex sinusoidal grating, modulated by a 2D Gaussian envelope. In a 2D coordinate (a, b) system, GF includes an imaginary and a real component, as given herewith:

$$G_{\delta,\theta,\psi,\sigma,\gamma}(a,b) = \exp\left(-\frac{a'^2+\gamma^2 b'^2}{2\sigma^2}\right) \times \exp\left(j\left(2\pi\frac{a'}{\delta}+\psi\right)\right) \quad (1)$$

in which:

$$a' = a\cos\theta + b\sin\theta \quad (2)$$

$$b' = -a\sin\theta + b\cos\theta \quad (3)$$

Now, δ characterizes the wavelength of sinusoidal factors, and θ signifies the orientation separation angle of the Gabor kernel. Consider θ in the interval $[0^\circ, 180^\circ]$, since the symmetry makes other directions redundant. ψ denotes the phase offset, σ indicates the standard derivation of the Gaussian envelope, and $\psi = 0$ and $\psi = \pi/2$ return the real and imaginary parts of Gabor filter, correspondingly. Variable 0 is defined by 6, and the spatial frequency bandwidth '*bw*' is determined as follows.

$$\sigma = \frac{\delta}{pi}\sqrt{\frac{ln2}{2}}\frac{2^{bw}+1}{2^{bw}-1} \quad (4)$$

3.2. Feature Extraction

At this stage, the NASNetLarge model performs a feature extraction process on the pre-processed images [19]. Generally, a NASNet is a CNN model derived from a scalable NAS model and reinforcement learning. There is a parent AI named the recurrent neural network (RNN), or "The Controller", which examines the performance of the child AI "Child Network" in CNN. Further, it also regulates the architecture of the "Child Network". These changes are accomplished on numerous layers, while regularization approaches, weights, etc., are utilized to enhance the performance of the "Child Network". It is trained on two distinct image sizes to form two kinds of NASNet models, namely NASNetLarge and NASNetMobile. Each NASNet model holds a fundamental element called a block. A cell is an arrangement of blocks, and is designed by the concatenation of different operational blocks. Numerous cells create the NASNet architecture. The controller RNN enhances the cells with blocks, and is undefined because it is optimized for a selected dataset. Each block is an operational module, and the operations that can be performed by a block are given herewith:

- Convolution;
- Max-Pooling;
- Average-Pooling;
- Separable Convolutions; and
- Identity Mapping.

The NASNet-Large approach comprises of encoding as well as decoding units that are trailed by a classifier layer. The NASNet-Large-decoding network makes use of the initial 414 layers of the NASNet-Large net, whereas the encoding unit is applied for image decomposition. An initial set of 414 layers is used, owing to the fact that the final layer size is closer to input image size. When the final layer is chosen for the feature extraction process, it can abolish the important structural data about objects, since the final layer is responsible for classification. The non-availability of pre-trained weights retrains the network with the help of new data. Here, the pooling layer is not available in the decoding unit, since it can offer detailed information to the decoding unit. A proper decoding unit can upsample the input feature map with the help of a max pooling layer. The decoding unit includes a set of four blocks. Every individual block starts with upsampling that could

extend the feature map, trailed by convolutional and rectified linear units. Moreover, batch normalization is employed for every individual map. The initial decoding unit, closer to the final encoding unit, can produce multi-channel feature amp. The end outcome of the final decoding layer is passed onto the WELM classification model, which generates a K channel image of likelihoods, where K indicates the class count.

3.3. Image Classification Using the WELM Model

In this study, the WELM model is exploited for lung nodule classification [20]. An extreme learning machine (ELM) is employed for the classification of a balanced dataset, whereas WELM is applied for the classification for imbalanced dataset. The training dataset has N distinct instances, $(x_i,\ z_i), i = 1, 2, \ldots, N$. A single hidden layer (HL) and a neural network (NN) with L HL nodes are expressed herewith:

$$\sum_{i=1}^{L} \beta_i \cdot 1(w_i \cdot x_j + b_i) = z_j, j = 1, \ldots, N \tag{5}$$

Whereas $l()$ indicates the activation function, w_i signifies a single HL input weight, β_i denotes the output weight, and b_i denotes single HLs bias, which are described below.

$$S\beta = T \tag{6}$$

Here, S denotes the resultant matrix of single HL.

$$S(w_1,\ \ldots,\ w_L,\ b_1,\ \ldots,\ b_L,\ x_1,\ \ldots,\ x_N) = \begin{pmatrix} l(w_1 \cdot x_1 + b_1) & \cdots & l(w_L \cdot x_1 + b_L) \\ \vdots & \ddots & \vdots \\ l(w_1 \cdot x_N + b_1) & \cdots & l(w_L \cdot x_N + b_L) \end{pmatrix}_{N \times L} \tag{7}$$

Based on the Karush–Kuhn-Tucker concept, the Lagrangian factor is identified in changing the trained ELM as many problems are being handled. The resultant weight β is evaluated by the following equation:

$$\beta = S^T \left(\frac{1}{C} + SS^T \right)^{-1} T \tag{8}$$

Now, C indicates the regularization coefficient. Henceforth, the output function of ELM classification is expressed below:

$$F(x) = s(x)S^T \left(\frac{1}{C} + SS^T \right)^{-1} T = \begin{bmatrix} K(x, x_1) \\ \vdots \\ K(x, x_N) \end{bmatrix}^T \left(\frac{1}{C} + \chi \right)^{-1} T \tag{9}$$

whereas χ represents the kernel matrix that is evaluated, as given below.

$$\chi = SS^T = s(x_i)s(x_j) = K(x_i,\ x_j) \tag{10}$$

It is obvious that the HL feature maps $s(x)$ denote the independence in classification outcome of ELM. Figure 2 demonstrates the infrastructure of ELM. The classification outcome was compared with the kernel function, $K(x,\ y)$. $K(x,\ y)$ considers an inner product process as follows:

$$K(x,\ y) = \exp\left(-\gamma \|x - y\|^2 \right) \tag{11}$$

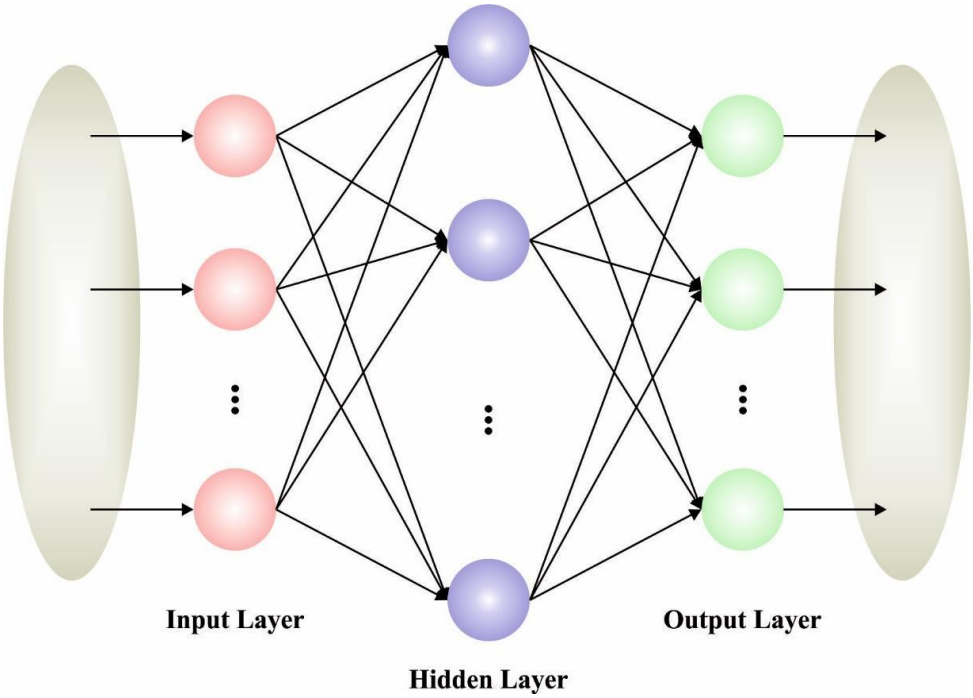

Figure 2. ELM structure.

Therefore, the kernel extreme learning machine (KELM) classification efficacy was distributed as to two parameters, namely the kernel function parameter, γ, and the penalty parameter, C. The original benefit of ELM is accomplished in WELM by preserving the weight for distinct instances to handle imbalanced classification problems. It is defined through the following equation:

$$F(x) = \begin{bmatrix} K(x, x_1) \\ \vdots \\ K(x, x_N) \end{bmatrix}^{\mathrm{T}} \left(\frac{1}{C} + W\chi \right)^{-1} WT, \tag{12}$$

$$W = diag\ (w_{ii}), i = 1, 2, \ldots, N \tag{13}$$

Here, W characterizes the weighted matrix. WELM has two weightage models as given herewith:

$$w_{ii} = \frac{1}{\#(z_i)}, \tag{14}$$

$$w_{ii} = \begin{cases} \frac{0.618}{\#(z_i)}, \ if z_i > \overline{z} \\ \frac{1}{\#(z_i)}, \ otherwise \end{cases} \tag{15}$$

Now, $\#(z_i)$ denotes the count of instances, going to class z_i, $i = 1, \ldots, m$. m indicates the count of classes. $\overline{z}$ denotes the average of complete instance.

3.4. Parameter Optimization Using the CSO Algorithm

In this final stage, the CSO algorithm is utilized for optimal parameter tuning of the WELM model, thereby producing an improved classification performance. The CSO approach is based on two major features of the cats [21], such as resting and hunting. During the resting skill, the cat spends their time resting, while it remains alert and slowly move to another position. However, when a target is recognized, the cat captures the target. Hence, an arithmetical model is designed to resolve difficult optimization problems and is named after the CSO algorithm. In this algorithm, tracing and seeking modes are defined to determine the behavior of cats. The working process of this mode are described herewith.

3.4.1. Seeking Mode

This model defines the resting skill of the cat. Here, a cat moves toward distinct locations in their searching space; in spite of this, it remains alert. It could be interpreted as a local search for the solution. The succeeding notation is utilized under this model.

- Seeking Memory Pool (SMP): it defines the number of copies of the cat being replicated.
- Seeking Range of selected dimension (SRD): it represents the variance between newer and older dimensions of the cat chosen for mutation.
- Count of Dimension to Change (CDC): it signifies the number of dimensions of a cat's location, experienced for mutation.

The stages of seeking mode of CSO are shown below.

1. Determine the count of copies (T) of *i*th cat. Based on the CDC parameter, subtract or add the SRD value arbitrarily from the existing location of cats, and replace the older value for each copy.
2. Calculate the fitness for each copy.
3. Select the optimal candidate solution and deploy at the location of *i*th cat.

3.4.2. Tracing Mode

Tracing mode reflects the hunting skill of the cat. Once the cat hunts the prey, both the velocity and the position of the cat are upgraded. Hence, a large variance takes place between newer and older locations of the cat. The velocity (V_j^d) and position (X_j^d) of jth cat in D—dimension space is determined by $X_j^d = \{X_j^1, X_j^2, \ldots\ldots X_j^D\}; V_j^d = \{V_j^1, V_j^2, \ldots\ldots V_j^D\}$; whereas $d = 1, 2, \ldots$ The optimal location of the cat is denoted by $X_{best}^d = \{X_{best}^1, X_{best}^2, \ldots\ldots X_{best}^D\}$. Both the velocity and position of jth cat is calculated using the following equation:

$$V_{jnew}^d = w * V_j^d + c * r * \left(X_{jbest}^d - X_j^d\right) \tag{16}$$

Whereas w represents a weight factor between 0 and 1, V_{jnew}^d characterizes the upgraded velocity of jth cat in dth dimension, c is a user-determined constant, V_j^d signifies the older velocity of jth cat, X_{jbest}^d characterizes the optimal location accomplished by jth cat in dth dimension, r signifies an arbitrary value between [0, 1], and X_j^d represents the existing location of jth cat in dth dimension, whereas $d = 1, 2, \ldots D$.

$$X_{jnew}^d = X_j^d + V_j^d \tag{17}$$

Now, X_j^d signifies the existing location of jth cat in dth dimension, V_j^d embodies the velocity of jth cat, *and* X_{jnew}^d signifies the upgraded location of jth cat in dth dimension. A mixture ratio (MR) is utilized to combine seek and trace modes. An MR is developed to describe the count of cats in seek and trace modes.

The CSO approach resolves an FF to achieve an enhanced classifier performance. It defines a positive integer for representing the optimum performance of candidate solutions. During this work, the minimal classifier error rate is regarded as FF, as provided in Equation (18). The optimum solution is a low error rate, and poor outcome gains an enhanced error rate.

$$fitness(x_i) = ClassifierErrorRate(x_i) = \frac{number\ of\ misclassified\ samples}{Total\ number\ of\ samples} * 100 \tag{18}$$

4. Experimental Validation

The proposed model was simulated using Python 3.6.5 tool with additional packages, such as tensorflow (GPU-CUDA Enabled), keras, numpy, pickle, matplotlib, sklearn, pillow,

and opencv-python. The simulation process was conducted on a PC with configurations, such as MSI Z370 A-Pro, i5-8600k, NVIDIA TITAN X, 16GB RAM, 250GB SSD, and 1TB HDD. The parameter settings are given as follows: batch size: 64, number of epochs: 15, learning rate: 0.05, dropout rate: 0.25, and activation function: rectified linear unit (ReLU).

The experimental validation of the proposed CSO-CADLCC model was conducted upon a benchmark lung database [22] that comprises a total of 300 images. In total, three class labels exist in the database, namely normal, benign, and malignant. Some sample images are depicted in Figure 3. The number of images under each class is 100.

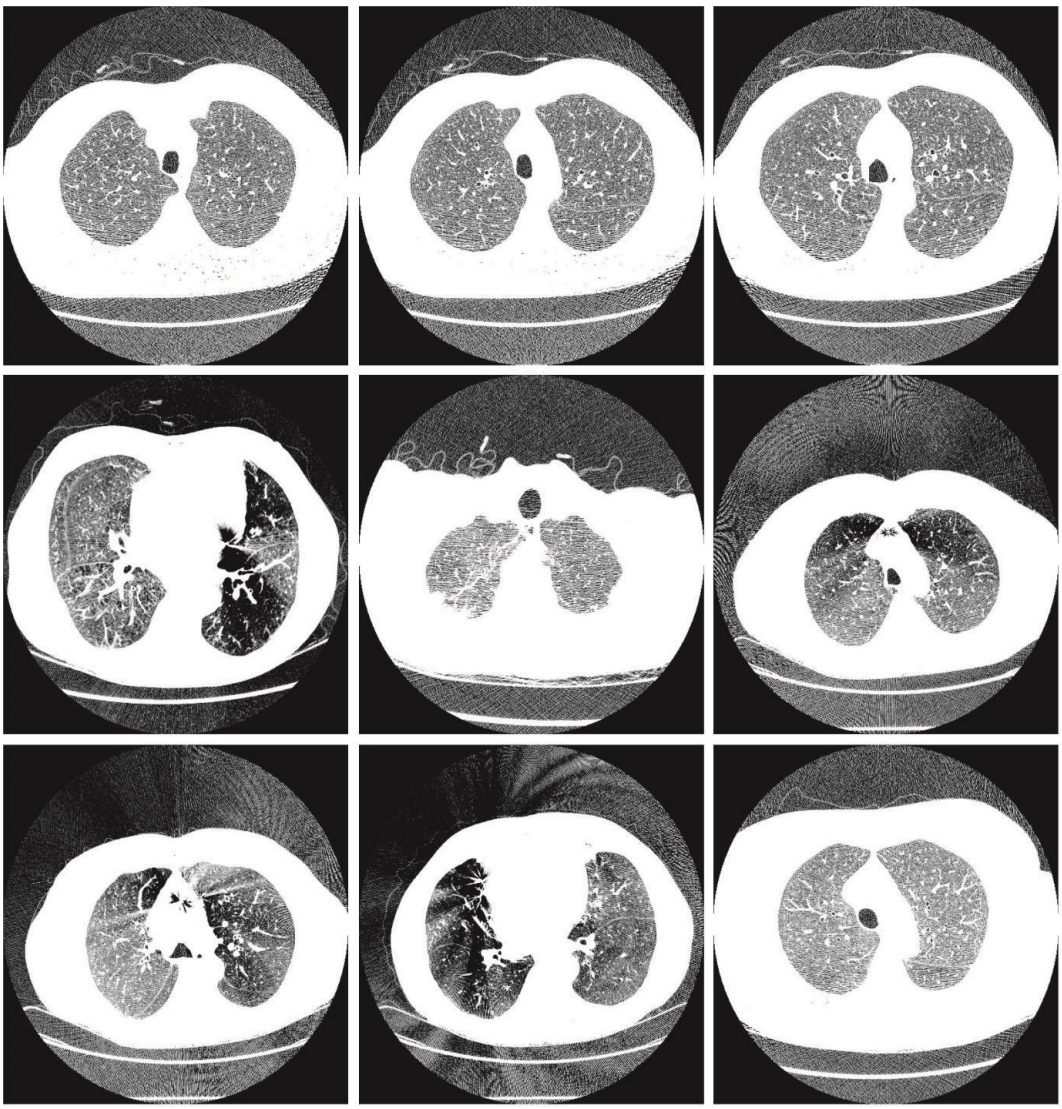

Figure 3. Sample Images.

Figure 4 demonstrates the confusion matrices generated by the CSO-CADLCC model on the distinct sizes of training/testing (TR/TS) data. With TR/TS data of 90:10, the proposed CSO-CADLCC model categorized 7 images as normal, 8 images as malignant, and 14 images as benign. Moreover, with TR/TS data of 80:20, the CSO-CADLCC technique categorized 18 images as normal, 20 images as malignant, and 21 images as benign. Furthermore, with TR/TS data of 70:30, the presented CSO-CADLCC approach categorized 20 images as normal class, 28 images as malignant class, and 39 images as benign. Finally, with TR/TS data of 60:40, the proposed CSO-CADLCC system categorized 35 images as normal, 34 images as malignant, and 34 images as benign.

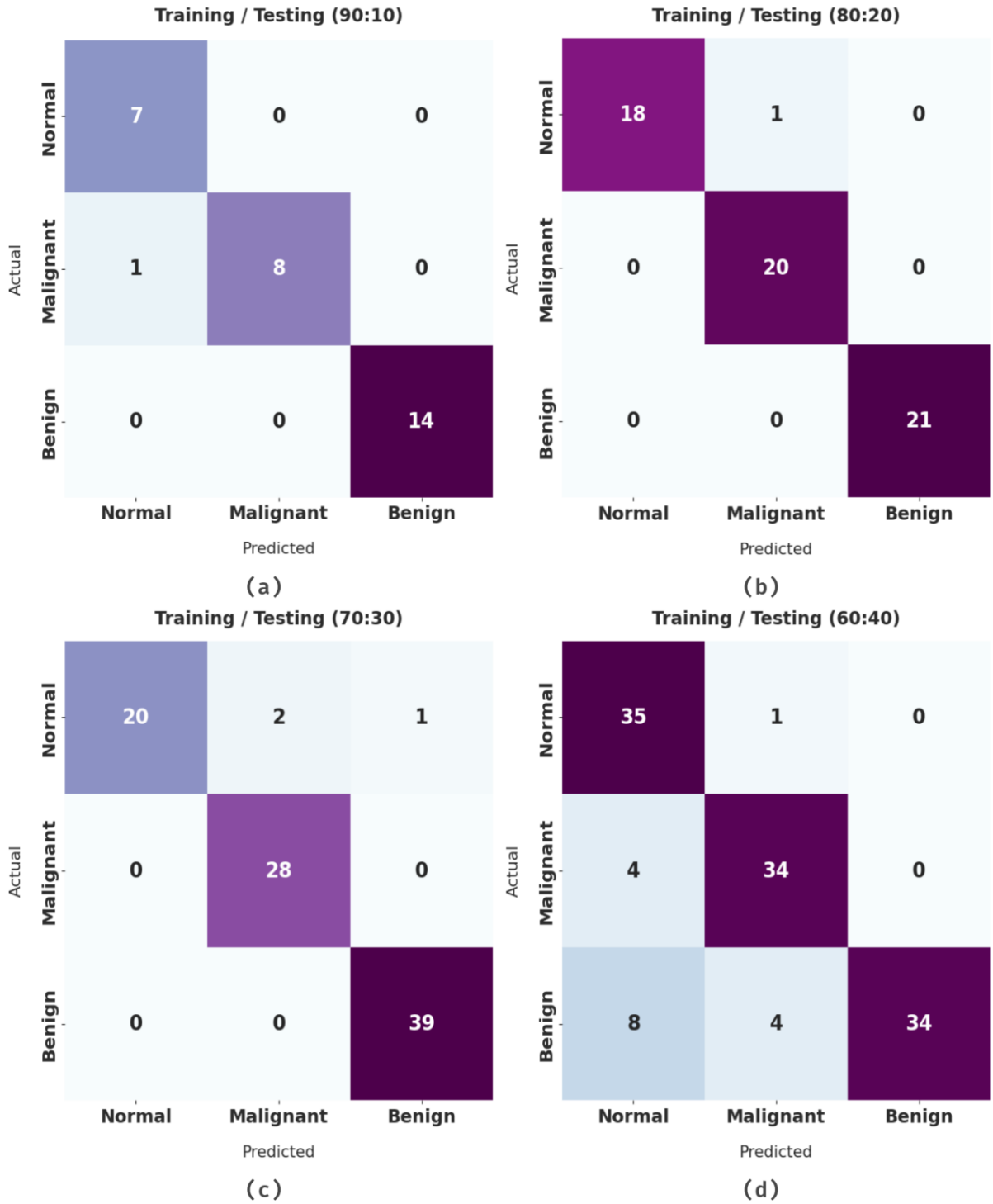

Figure 4. Confusion matrix of the CSO-CADLCC technique on distinct sizes of training/testing dataset. (**a**) TR/TS data of 90:10, (**b**) TR/TS data of 80:20, (**c**) TR/TS data of 70:30, and (**d**) TR/TS data of 60:40.

Table 1 and Figure 5 illustrate a brief overview of lung cancer classification results produced by the CSO-CADLCC model under distinct classes and TR/TS data. The experimental outcomes imply that the CSO-CADLCC model accomplished a maximum performance under all TR/TS data ratios. For instance, with 90:10 TR/TS data ratio, the proposed CSO-CADLCC model achieved an average $accu_y$, $prec_n$, $reca_l$, $spec_y$, F_{score}, and MCC of 97.78%, 95.83%, 96.30%, 98.55%, 95.82%, and, 94.53% respectively. Moreover, with

TR/TS data of 80:20, the CSO-CADLCC approach achieved an average $accu_y$, $prec_n$, $reca_l$, $spec_y$, F_{score}, and MCC of 98.89%, 98.41%, 98.25%, 99.17%, 98.29% and, 97.51%, respectively.

Table 1. Analysis results of the CSO-CADLCC technique under distinct classes and TR/TS data.

Class Labels	Accuracy	Precision	Recall	Specificity	F-Score	MCC
Training/Testing (90:10)						
Normal	96.67	87.50	100.00	95.65	93.33	91.49
Malignant	96.67	100.00	88.89	100.00	94.12	92.11
Benign	100.00	100.00	100.00	100.00	100.00	100.00
Average	97.78	95.83	96.30	98.55	95.82	94.53
Training/Testing (80:20)						
Normal	98.33	100.00	94.74	100.00	97.30	96.17
Malignant	98.33	95.24	100.00	97.50	97.56	96.36
Benign	100.00	100.00	100.00	100.00	100.00	100.00
Average	98.89	98.41	98.25	99.17	98.29	97.51
Training/Testing (70:30)						
Normal	96.67	100.00	86.96	100.00	93.02	91.23
Malignant	97.78	93.33	100.00	96.77	96.55	95.04
Benign	98.89	97.50	100.00	98.04	98.73	97.77
Average	97.78	96.94	95.65	98.27	96.10	94.68
Training/Testing (60:40)						
Normal	89.17	74.47	97.22	85.71	84.34	77.86
Malignant	92.50	87.18	89.47	93.90	88.31	82.81
Benign	90.00	100.00	73.91	100.00	85.00	79.75
Average	90.56	87.22	86.87	93.21	85.88	80.14

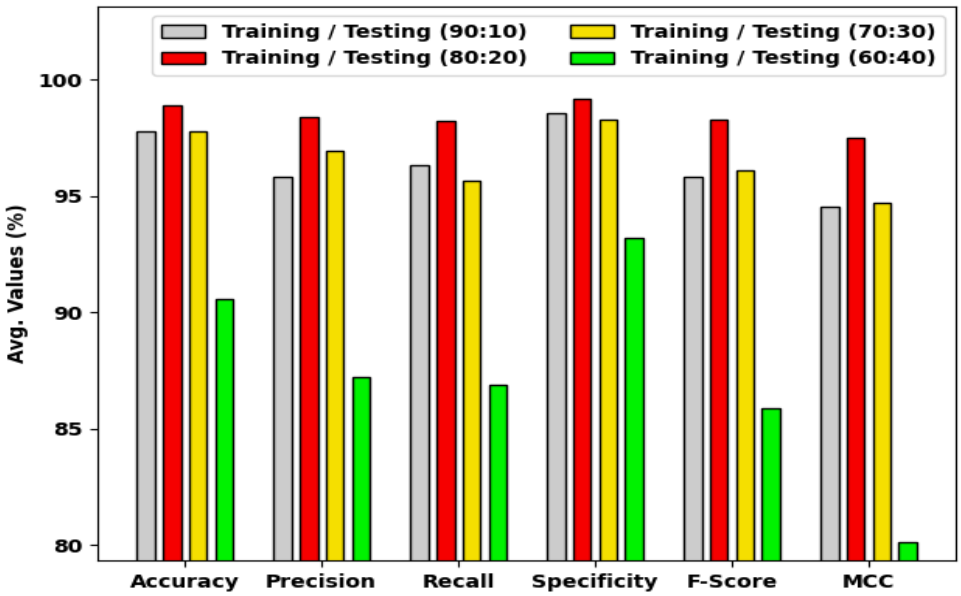

Figure 5. Analysis results of the CSO-CADLCC technique under distinct classes and TR/TS data.

Furthermore, with TR/TS data of 70:30, the proposed CSO-CADLCC approach accomplished an average $accu_y$, $prec_n$, $reca_l$, $spec_y$, F_{score}, and MCC of 97.78%, 96.94%, 95.65%,

98.27%, 96.10%, and, 94.68% respectively. In addition, with TR/TS data of 60:40, the presented CSO-CADLCC technique obtained an average $accu_y$, $prec_n$, $reca_l$, $spec_y$, F_{score}, and MCC of 90.56%, 87.22%, 86.87%, 93.21%, 85.88%, and, 80.14%, respectively.

Figure 6 illustrates a set of training and validation accuracy/loss graphs generated by the proposed CSO-CADLCC model under distinct TR/TS data. From these figures, it can be understood that the validation accuracy is higher and the validation loss is lower, compared to the training accuracy/loss.

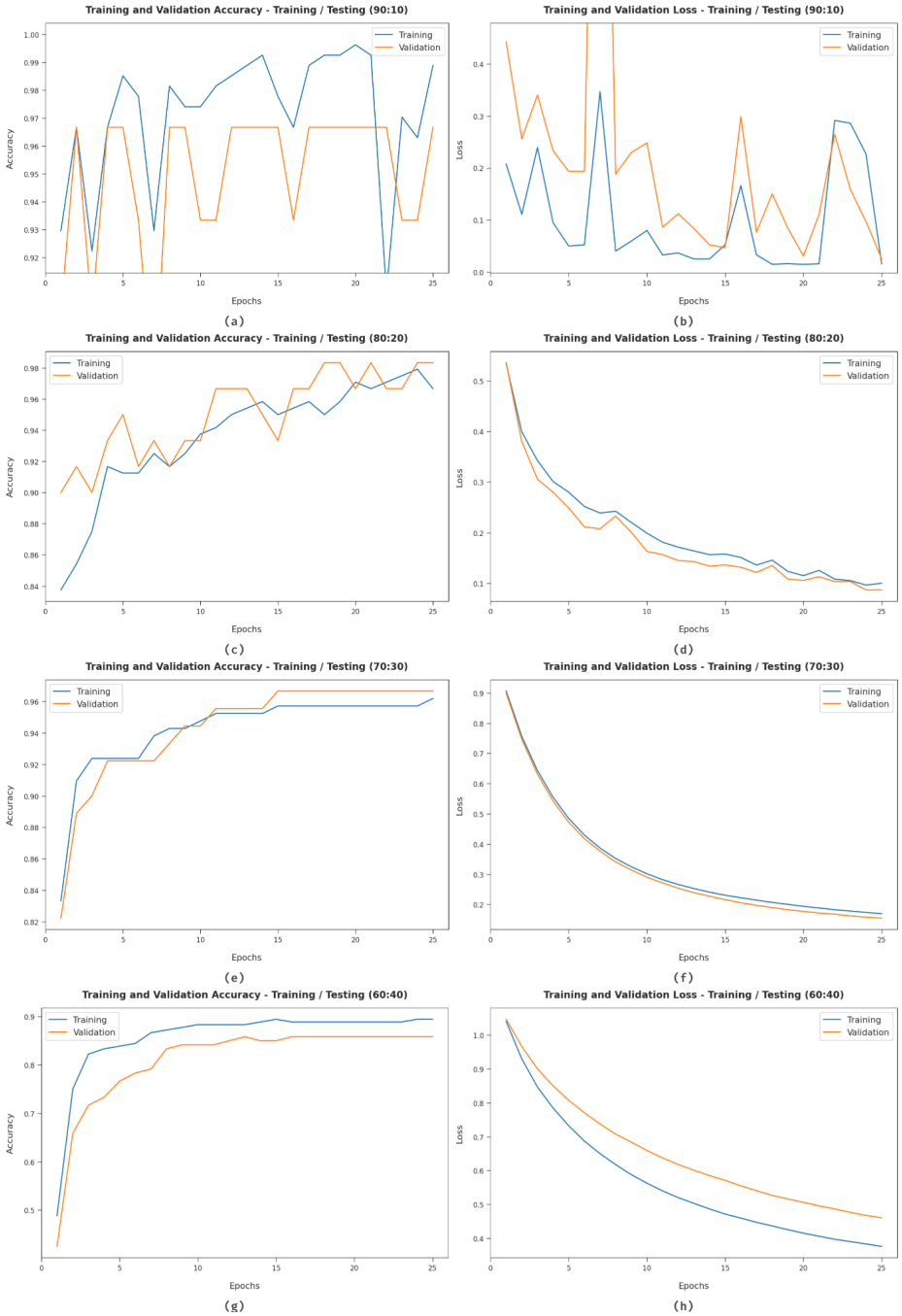

Figure 6. Accuracy and loss analyses results of the CSO-CADLCC technique under distinct TR/TS data. (**a**) TA/VA data of 90:10, (**b**) TL/VL data of 90:10, (**c**) TA/VA data of 80:20, (**d**) TL/VL data of 80:20, (**e**) TA/VA data of 70:30, (**f**) TL/VL data of 70:30, (**g**) TA/VA data of 60:40, (**h**) TL/VL data of 60:40.

Figure 7 reports the precision–recall curve analysis results accomplished by the CSO-CADLCC model under distinct TR/TS data. The figures indicate that the proposed CSO-CADLCC model produced effectual outcomes under distinct TR/TS data.

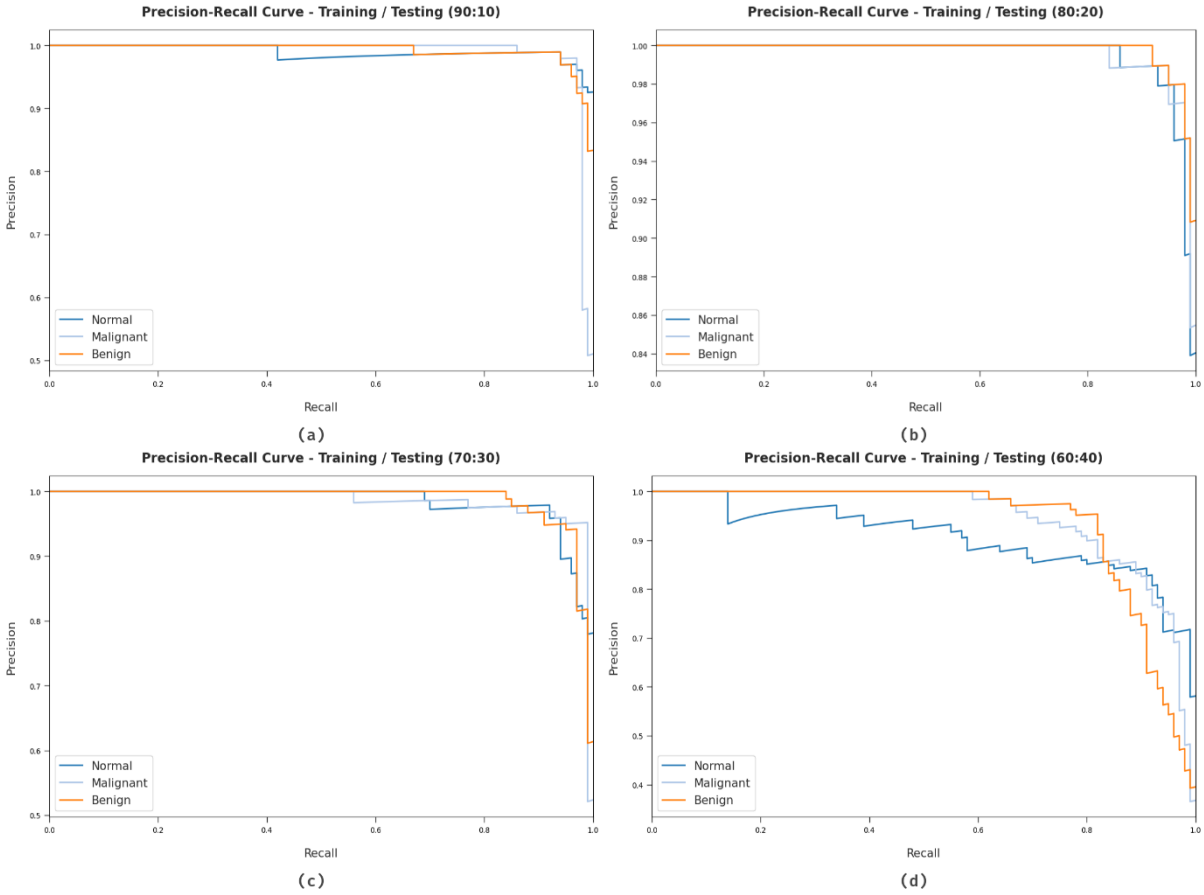

Figure 7. Precision–recall analysis results of the CSO-CADLCC technique under distinct TR/TS data. (**a**) TR/TS data of 90:10, (**b**) TR/TS data of 80:20, (**c**) TR/TS data of 70:30, and (**d**) TR/TS data of 60:40.

Table 2 reports extensive lung cancer classification outcomes achieved by the proposed CSO-CADLCC model and other existing models [23,24]. Figure 8 compares the $accu_y$ values achieved by the CSO-CADLCC model and other recent models. The figure indicates that the AlexNet model achieved poor results with low $accu_y$. At the same time, the ResNet5-SVM and AlexNet models depicted slightly improved $accu_y$ values. Furthermore, the optimal-DNN, artificial neural network (ANN), multi-class CNN (MC-CNN), CNN, and visual geometry group (VGG16) models demonstrated reasonable $accu_y$ values. However, the proposed CSO-CADLCC model outperformed all other methods, and achieved a maximum $accu_y$ of 98.89%.

Figure 9 portrays the comparative analysis results in terms of $prec_n$, $reca_l$, $spec_y$, and F_{score} achieved by the CSO-CADLCC approach against existing methods. The figure demonstrates that the AlexNet approach achieved the least outcomes, with lesser values of $prec_n$, $reca_l$, $spec_y$, and F_{score}. Moreover, the ResNet5-SVM and AlexNet techniques demonstrated somewhat enhanced values of $prec_n$, $reca_l$, $spec_y$, and F_{score}. Furthermore, the optimal-DNN, ANN, MC-CNN, CNN, and VGG16 techniques have accomplished reasonable values of $prec_n$, $reca_l$, $spec_y$, and F_{score}. Eventually, the proposed CSO-CADLCC approach outperformed all other approaches, with maximal $prec_n$, $reca_l$, $spec_y$, and F_{score} values of 98.41%, 98.25%, 99.17%, and 98.29%, respectively.

Table 2. Comparative analysis between the CSO-CADLCC technique and other recent algorithms.

Methods	Accuracy	Precision	Recall	Specificity	F-Score
Optimal-DNN	97.81	97.73	97.68	97.54	95.15
Artificial NN	97.17	95.02	95.72	96.29	96.46
MC-CNN	97.78	95.43	97.72	97.58	95.77
CNN	97.87	96.92	95.26	96.61	95.73
ResNet50-SVM	96.30	97.67	96.68	96.54	96.60
AlexNet	95.50	97.36	97.34	95.83	95.65
VGG16	97.99	95.30	96.48	97.11	97.26
CSO-CADLCC	98.89	98.41	98.25	99.17	98.29

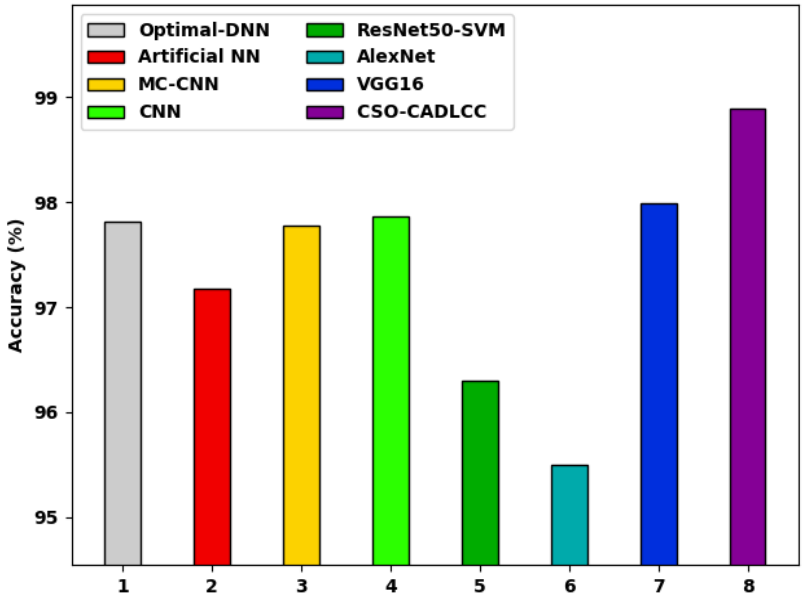

Figure 8. Accuracy analysis of the CSO-CADLCC technique with recent algorithms.

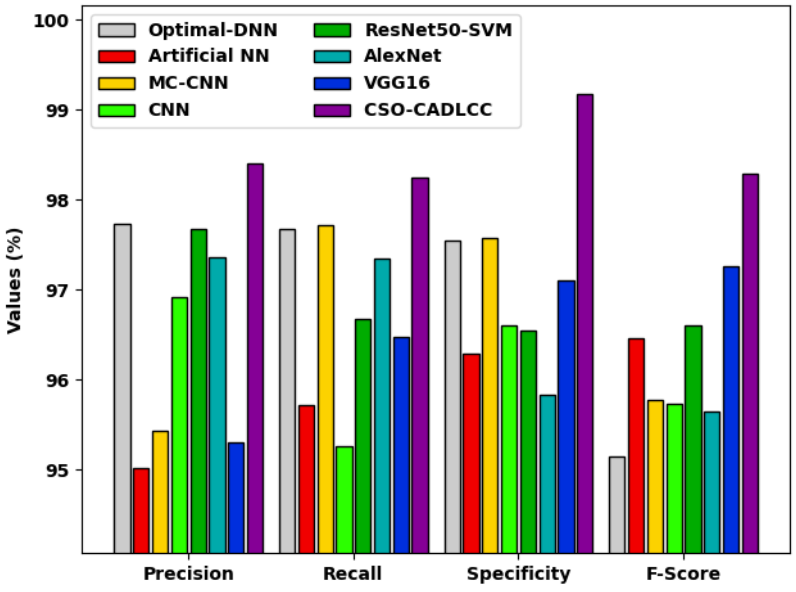

Figure 9. Comparative analysis of the CSO-CADLCC technique with recent algorithms.

A detailed running time (RT) and training time (TT) analysis was conducted between the CSO-CADLCC model and recent models, and the results are shown in Table 3 and Figure 10. The results imply that the optimal DNN model offered a poor performance with a maximum RT of 10.55 s. At the same time, the ANN, MC-CNN, CNN, and ResNet50-SVM models obtained slightly decreased RT values of 9.97 s, 9.13 s, 8.66 s, and 7.99 s, respectively. Moreover, the AlexNet and VGG16 models resulted in reasonable RT values of 5.92 s and 3.38 s, respectively. However, the proposed CSO-CADLCC model accomplished the maximum performance by achieving the lowest RT of 1.68 s. At the same time, it can also be noted that the proposed model underwent the lowest training time of 21.54 min, whereas the optimal DNN model underwent the maximum training time of 58.45 min.

Table 3. Running time and training time analysis results of the CSO-CADLCC approach with recent methods.

Methods	Running Time (s)	Training Time (Min)
Optimal-DNN	10.55	58.45
Artificial NN	9.97	47.24
MC-CNN	9.13	42.07
CNN	8.66	36.24
ResNet50-SVM	7.99	34.89
AlexNet	5.92	29.54
VGG16	3.38	25.48
CSO-CADLCC	1.68	21.54

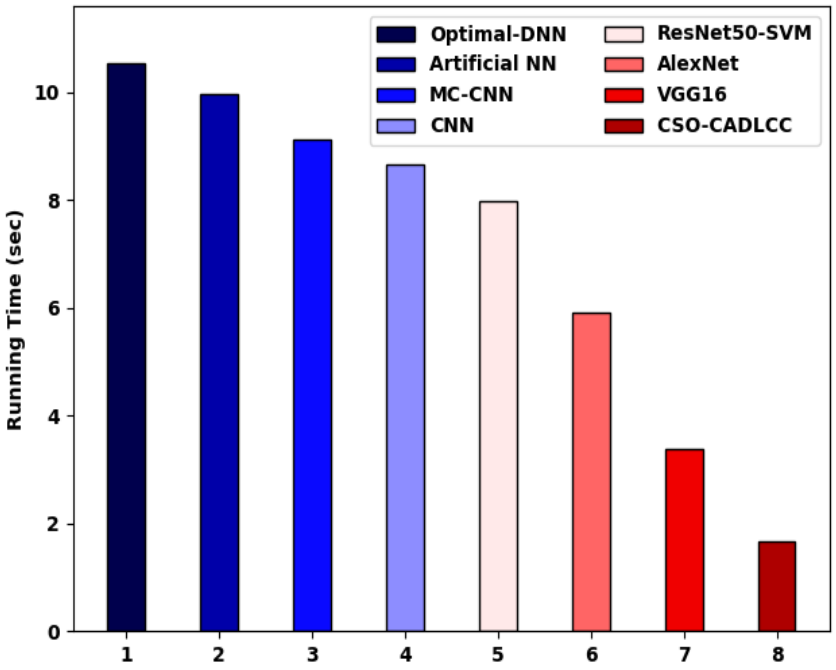

Figure 10. RT analysis results of the CSO-CADLCC approach with recent approaches.

Based on the aforementioned results and discussion, it can be inferred that the CSO-CADLCC methodology achieved the maximum performance in lung cancer classification.

5. Conclusions

In this article, a new CSO-CADLCC model has been developed for the identification and classification of lung cancer using CT images. The presented CSO-CADLCC

model comprises of a GF technique to eradicate the noise at preliminary stage. Then, a NASNetLarge model is utilized for a feature extraction process on pre-processed images. Furthermore, a WELM model is exploited for the classification of lung nodules. Finally, a CSO algorithm is utilized for optimal parameter tuning of the WELM model, which results in an improved classification performance. The CSO-CADLCC technique was experimentally validated against a benchmark dataset, and the results were assessed under several aspects. The simulation results indicate that the proposed model achieved a better performance over existing approaches under different measures. In the future, deep instance segmentation models can be employed to improve lung cancer classification performance. In addition, an ensemble of fusion-based DL models can be applied to enhance the detection efficiency of the proposed model. Moreover, the proposed model can also be tested on large scale datasets in the future.

Author Contributions: Conceptualization, T.V.; Data curation, L.; Formal analysis, L.; Investigation, H.A.; Methodology, T.V. and H.A.; Resources, R.P. and A.H.; Software, R.P. and A.H.; Validation, V.P.; Visualization, V.P. and A.H.; Writing—original draft, T.V.; Writing—review & editing, H.A. All authors have read and agreed to the published version of the manuscript.

Funding: This work is funded by Deanship of Scientific Research at Prince Sattam Bin Abdulaziz University (Project No 2020/01/1174).

Institutional Review Board Statement: Not applicable.

Informed Consent Statement: Not applicable.

Data Availability Statement: Data sharing is not applicable to this article, as no datasets were generated during the current study.

Acknowledgments: The authors would like to thank Prince Sattam Bin Abdualziz University for providing the technical support during this research work. This project was supported by the Deanship of Scientific Research at Prince Sattam Bin Abdulaziz University (project no. 2020/01/1174).

Conflicts of Interest: The authors declare that they have no conflict of interest. The manuscript was written with the contributions of all authors. All authors have given approval to the final version of the manuscript.

References

1. Zhang, S.; Sun, F.; Wang, N.; Zhang, C.; Yu, Q.; Zhang, M.; Babyn, P.; Zhong, H. Computer-aided diagnosis (CAD) of pulmonary nodule of thoracic CT image using transfer learning. *J. Digit. Imaging* **2019**, *32*, 995–1007. [CrossRef] [PubMed]
2. Nishio, M.; Nishio, M.; Jimbo, N.; Nakane, K. Homology-based image processing for automatic classification of histopathological images of lung tissue. *Cancers* **2021**, *13*, 1192. [CrossRef] [PubMed]
3. Arshad, M.; Khan, M.A.; Tariq, U.; Armghan, A.; Alenezi, F.; Younus Javed, M.; Aslam, S.M.; Kadry, S. A Computer-Aided Diagnosis System Using Deep Learning for Multiclass Skin Lesion Classification. *Comput. Intell. Neurosci.* **2021**, *2021*, 9619079. [CrossRef] [PubMed]
4. Agarwal, A.; Patni, K.; Rajeswari, D. Lung cancer detection and classification based on alexnet CNN. In Proceedings of the 2021 6th International Conference on Communication and Electronics Systems (ICCES), Coimbatore, India, 8–10 July 2021; IEEE: New York, NY, USA, 2021; pp. 1390–1397.
5. Zebari, D.A.; Ibrahim, D.A.; Zeebaree, D.Q.; Haron, H.; Salih, M.S.; Damaševičius, R.; Mohammed, M.A. Systematic Review of Computing Approaches for Breast Cancer Detection Based Computer Aided Diagnosis Using Mammogram Images. *Appl. Artif. Intell.* **2021**, *35*, 1–47. [CrossRef]
6. Calheiros, J.L.L.; de Amorim, L.B.V.; de Lima, L.L.; de Lima Filho, A.F.; Ferreira Júnior, J.R.; de Oliveira, M.C. The effects of perinodular features on solid lung nodule classification. *J. Digit. Imaging* **2021**, *34*, 798–810. [CrossRef]
7. Binczyk, F.; Prazuch, W.; Bozek, P.; Polanska, J. Radiomics and artificial intelligence in lung cancer screening. *Transl. Lung Cancer Res.* **2021**, *10*, 1186. [CrossRef]
8. Wu, J.; Gou, F.; Tan, Y. A staging auxiliary diagnosis model for nonsmall cell lung cancer based on the intelligent medical system. *Comput. Math. Methods Med.* **2021**, *2021*, 6654946. [CrossRef]
9. Mohan, B.P.; Khan, S.R.; Kassab, L.L.; Ponnada, S.; Chandan, S.; Ali, T.; Dulai, P.S.; Adler, D.G.; Kochhar, G.S. High pooled performance of convolutional neural networks in computer-aided diagnosis of GI ulcers and/or hemorrhage on wireless capsule endoscopy images: A systematic review and meta-analysis. *Gastrointest. Endosc.* **2021**, *93*, 356–364. [CrossRef]

10. Li, X.; Li, C.; Rahaman, M.M.; Sun, H.; Li, X.; Wu, J.; Yao, Y.; Grzegorzek, M. A comprehensive review of computer-aided whole-slide image analysis: From datasets to feature extraction, segmentation, classification and detection approaches. *Artif. Intell. Rev.* **2022**, 1–70. [CrossRef]
11. Hu, X.; Gong, J.; Zhou, W.; Li, H.; Wang, S.; Wei, M.; Peng, W.; Gu, Y. Computer-aided diagnosis of ground glass pulmonary nodule by fusing deep learning and radiomics features. *Phys. Med. Biol.* **2021**, *66*, 065015. [CrossRef]
12. Lu, H. Computer-aided diagnosis research of a lung tumor based on a deep convolutional neural network and global features. *BioMed Res. Int.* **2021**, *2021*, 5513746. [CrossRef] [PubMed]
13. Guo, Z.; Xu, L.; Si, Y.; Razmjooy, N. Novel computer-aided lung cancer detection based on convolutional neural network-based and feature-based classifiers using metaheuristics. *Int. J. Imaging Syst. Technol.* **2021**, *31*, 1954–1969. [CrossRef]
14. Ali, I.; Muzammil, M.; Haq, I.U.; Khaliq, A.A.; Abdullah, S. Deep feature selection and decision level fusion for lungs nodule classification. *IEEE Access* **2021**, *9*, 18962–18973. [CrossRef]
15. Mastouri, R.; Khlifa, N.; Neji, H.; Hantous-Zannad, S. A bilinear convolutional neural network for lung nodules classification on CT images. *Int. J. Comput. Assist. Radiol. Surg.* **2021**, *16*, 91–101. [CrossRef]
16. Shaffie, A.; Soliman, A.; Eledkawy, A.; van Berkel, V.; El-Baz, A. Computer-Assisted Image Processing System for Early Assessment of Lung Nodule Malignancy. *Cancers* **2022**, *14*, 1117. [CrossRef]
17. Abid, M.M.N.; Zia, T.; Ghafoor, M.; Windridge, D. Multi-view convolutional recurrent neural networks for lung cancer nodule identification. *Neurocomputing* **2021**, *453*, 299–311. [CrossRef]
18. Chen, Y.; Zhu, L.; Ghamisi, P.; Jia, X.; Li, G.; Tang, L. Hyperspectral images classification with Gabor filtering and convolutional neural network. *IEEE Geosci. Remote Sens. Lett.* **2017**, *14*, 2355–2359. [CrossRef]
19. Zhang, Y.; Davison, B.D.; Talghader, V.W.; Chen, Z.; Xiao, Z.; Kunkel, G.J. Automatic Head Overcoat Thickness Measure with NASNet-Large-Decoder Net. In Proceedings of the Future Technologies Conference, Vancouver, BC, Canada, 28–29 November 2021; Springer: Cham, Switzerland, 2021; pp. 159–176.
20. Liu, Z.; Tang, D.; Cai, Y.; Wang, R.; Chen, F. A hybrid method based on ensemble WELM for handling multi class imbalance in cancer microarray data. *Neurocomputing* **2017**, *266*, 641–650. [CrossRef]
21. Ahmed, A.M.; Rashid, T.A.; Saeed, S.A.M. Cat swarm optimization algorithm: A survey and performance evaluation. *Comput. Intell. Neurosci.* **2020**, *2020*, 4854895. [CrossRef]
22. ELCAP Public Lung Image Database. Available online: http://www.via.cornell.edu/lungdb.html (accessed on 14 December 2021).
23. Lakshmanaprabu, S.K.; Mohanty, S.N.; Shankar, K.; Arunkumar, N.; Ramirez, G. Optimal deep learning model for classification of lung cancer on CT images. *Future Gener. Comput. Syst.* **2019**, *92*, 374–382.
24. Masud, M.; Sikder, N.; Nahid, A.A.; Bairagi, A.K.; AlZain, M.A. A machine learning approach to diagnosing lung and colon cancer using a deep learning-based classification framework. *Sensors* **2021**, *21*, 748. [CrossRef] [PubMed]